Fundamentals of Unmanned Aerial Vehicles Project

AER1216

Final Report

Shahzeb Mahmood - 1003017497
David Rolko - 1003037420
Farhan Wadia - 1003012606

Table of Contents

List of Figures

List of Tables

1.0 Overview

The goal of the AER1216 Project for Fall 2021 was to conduct performance analysis and develop simulation models for both a fixed-wing sUAS configuration and a multi-rotor drone configuration.

For the fixed-wing model, parameters for the Aerosonde UAV were provided. Using this data and the information about the propeller and engine, information about the optimal velocity, power, and fuel consumption was determined. This was used to calculate that the maximum range is approximately 4034 km and the maximum endurance is approximately 65 hr and 5 min. These values were observed to be quite large for the size of the UAV, and this was determined to be primarily due to inaccurate engine information used in the calculations. Furthermore, a simulation was developed in which the UAV was required to perform an ascent to 2000 m, a 180° turn, and a descent to 1000 m. Firstly, a linear state-space dynamics model was developed for the UAV using the aircraft data and the equations for the aerodynamic and control derivatives. Secondly, the dynamic model was used along with linear quadratic regulator (LQR) control to obtain gain matrices for the longitudinal and lateral modes. Thirdly, the control system was modelled in Simulink, along with a distance tracker to determine the UAVs north position in the Earth reference frame. This was a critical input for the logic function needed to decide the command input at each timestep. After running the simulation, it was observed that the UAS performed the required manoeuvres, but at unrealistic speeds and an unrealistic turn radius. Possible reasons for the discrepancy between the results and the expected behaviour include tuning inaccuracies and lack of saturation on control surface deflections.

Moreover, a 0th order battery model was used to calculate the maximum range and endurance for a multi-rotor configuration. The maximum range was determined to be 36.061 km at a speed of 9.5 m/s, and the maximum endurance was determined to be 68.1 min at a speed of 7 m/s. Given the state-space dynamics for the roll, pitch, yaw, height, pitch to u, and pitch to v, a dynamics model was implemented for the multi-rotor configuration. This was combined with position estimation and PID control to build the overall control model. The controller was designed in Simulink and the simulation yielded favourable results, as the multi-rotor was able to carry out the desired movements with relatively low error and overshoot.

A major lesson learned during the project is that design is all about tradeoffs. Optimising one particular parameter of the design may result in another parameter becoming suboptimal. For instance, during PID tuning, trying to reduce the settling time often resulted in an increase in overshoot or steady-state error.

2.0 Fixed-Wing sUAS Development

A study was conducted which modelled and simulated an Aerosonde UAV using MATLAB and Simulink. The maximum range and endurance performance was first calculated for the UAS. Furthermore, a controller was developed to execute a set of commands such as flying to a specific height and performing level-coordinated turns. The fixed wing dynamics model was first developed, then a control system was made to control the speed, altitude, and flight heading direction.

2.1 Fixed-Wing Range and Endurance

The maximum range and endurance were calculated for the UAV. Using information about the UAV, the propeller (16 x 8 carbon electric), and the engine (Lycoming EL-005), an estimate was calculated [1], [2]. The altitude was assumed to be approximately 500 m above sea-level which should provide some distance between the ground and the plane (varies with location). To find the range endurance of the plane, the inverse of the fuel rate of consumption (Ẇ) was integrated over the initial weight of the plane (with a full tank of fuel) to the final weight of the plane (an empty tank of fuel). To find the range, the same integral was used but multiplied by the velocity.

$$Endurance = \int_{w_{initial}}^{w_{final}} \frac{1}{fuel\,rate} dw \quad Range = \int_{w_{initial}}^{w_{final}} \frac{velocity}{fuel\,rate} dw$$

To find the max endurance, the minimal fuel rate of consumption needs to be determined and for the max range the max ratio of velocity over rate of fuel consumption needs to be determined. The fuel rate is a function of the power output of the engine. A linear fit was developed using the two data points given (see Figure 2-1). The power is a function of the velocity which the plane is flying at. The velocity of the plane influences the drag (and therefore the thrust required) and it also influences the "J" value of the propeller. To calculate the RPM which the propeller is spinning at, the "CT" coefficient and the "J" value need to be solved simultaneously. Using the data from the prop, a curve of best fit was applied to the data points (see Appendix A). To determine the ideal velocity to fly at, the fuel consumption and the fuel consumption over velocity were determined over a range of velocities (see Appendix B). The speeds that give the minimum values correspond to the optimal flight speed. Since the weight of the plane changes throughout the flight, this optimal velocity and corresponding fuel consumption is continuously updated with each iteration (see Figure 2-2).

Using this method, it was estimated that the maximum range is approximately 4034 km and the maximum endurance is approximately 65 hr and 5min. These values were considerably larger than expected for this UAV. After further analysis, it was determined that this is due to inaccurate information used in the calculations. The engine analysed is proportionally much too large for the plane used. The average power needed to spin the prop was 219 watts (at 5291 RPM) for range and 195 watts for endurance (at 4890 RPM). This results in a much smaller torque than the engine realistically provides. For example, even at flight idle the engine provides 450 watts (at

3200 RPM) [2]. As a result, the fuel consumption rate drops to very low unrealistic values, where the linear approximation is no longer accurate.

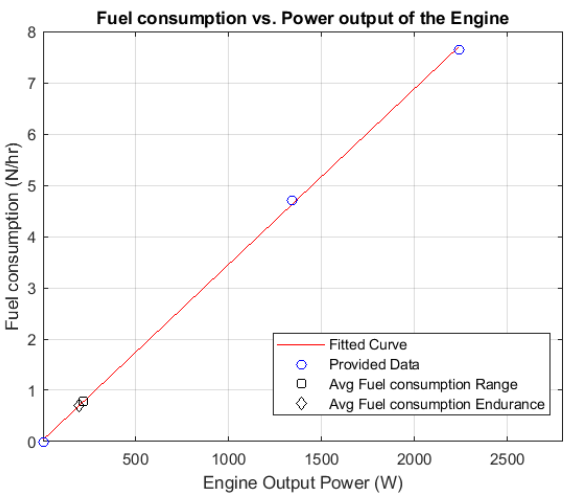

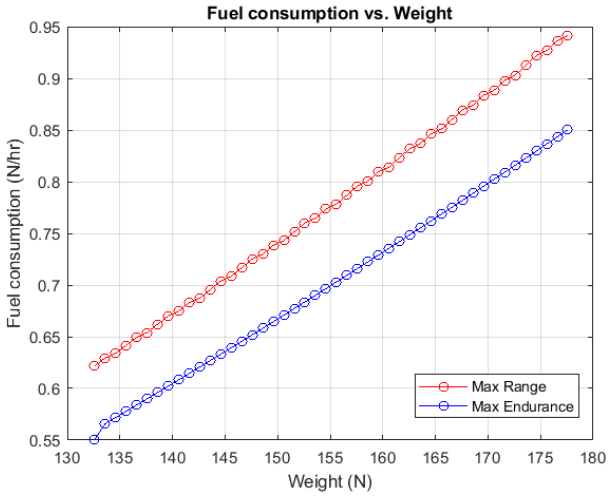

Figure 2-1: Fuel Consumption Per Power *Figure 2-2: Fuel Consumption Vs. Changing Weight*

These calculations also make several assumptions that increased the result from the range and endurance that would be expected in the field. The calculations try to find the max theoretical values where the speed is constantly being optimised which may not be realistic for actual flight. The model neglects the increased power to take-off and land, and it neglects disturbances such as wind which will further reduce the range and endurance. Finally, the model assumes that the power output of the engine is equal to the required propeller power, assuming that there are no energy losses in the shaft driving the prop.

2.2 Fixed-Wing Dynamics Modelling

The objective of the fixed wing model is to have the UAS perform an ascent to an altitude of 2000 m for 1000 m, perform a 180° turn with a turn radius of 250 m, then descend to an altitude of 2000 m. This translates to altitude hold and a coordinated turn. The linearized state-space equations were used to build the aircraft dynamics model. These equations are decoupled into longitudinal and lateral dynamics:

$$\dot{x} = A_{long}x + B_{long}u$$

$$\dot{x} = A_{latr}x + B_{latr}u$$

For the longitudinal dynamics, the speed, u, and the altitude, h are of interest. For the lateral dynamics, the roll angle, ϕ, and the yaw angle, ψ are of interest. The following equations were modelled in MATLAB:

$$\begin{pmatrix}\dot{\bar{u}}\\ \dot{\bar{w}}\\ \dot{\bar{q}}\\ \dot{\bar{\theta}}\\ \dot{\bar{h}}\end{pmatrix} = \begin{pmatrix} X_u & X_w & X_q & -g\cos\theta^* & 0\\ Z_u & Z_w & Z_q & -g\sin\theta^* & 0\\ M_u & M_w & M_q & 0 & 0\\ 0 & 0 & 1 & 0 & 0\\ \sin\theta^* - \cos\theta^* & 0 & u^*\cos\theta^* + w^*\sin\theta^* & 0 & \end{pmatrix}\begin{pmatrix}\bar{u}\\ \bar{w}\\ \bar{q}\\ \bar{\theta}\\ \bar{h}\end{pmatrix} + \begin{pmatrix} X_{\delta_e} & X_{\delta_t}\\ Z_{\delta_e} & 0\\ M_{\delta_e} & 0\\ 0 & 0\\ 0 & 0\end{pmatrix}\begin{pmatrix}\bar{\delta}_e\\ \bar{\delta}_t\end{pmatrix},$$

$$\begin{pmatrix}\dot{\bar{v}}\\ \dot{\bar{p}}\\ \dot{\bar{r}}\\ \dot{\bar{\phi}}\\ \dot{\bar{\psi}}\end{pmatrix} = \begin{pmatrix} Y_v & Y_p & Y_r & g\cos\theta^*\cos\phi^* & 0\\ L_v & L_p & L_r & 0 & 0\\ N_v & N_p & N_r & 0 & 0\\ 0 & 1 & \cos\phi^*\tan\theta^* & q^*\cos\phi^*\tan\theta^* - r^*\sin\phi^*\tan\theta^* & 0\\ 0 & 0 & \cos\phi^*\sec\theta^* & p^*\cos\phi^*\sec\theta^* - r^*\sin\phi^*\sec\theta^* & 0\end{pmatrix}\begin{pmatrix}\bar{v}\\ \bar{p}\\ \bar{r}\\ \bar{\phi}\\ \bar{\psi}\end{pmatrix} + \begin{pmatrix} Y_{\delta_a} & Y_{\delta_r}\\ L_{\delta_a} & L_{\delta_r}\\ N_{\delta_a} & N_{\delta_r}\\ 0 & 0\\ 0 & 0\end{pmatrix}\begin{pmatrix}\bar{\delta}_a\\ \bar{\delta}_r\end{pmatrix}, \quad [3]$$

where the X, Z, M, Y, L, N terms are the aerodynamic and control derivatives calculated from the aircraft parameters. The equation used to calculate the aerodynamic and control derivatives are available in Appendix C.

After computing the aerodynamic and control derivatives, the following matrices were obtained:

$$A_{long} = \begin{bmatrix} -0.1990 & 0 & 0 & -9.81 & 0\\ -1.531 & 0 & 15 & 0 & 0\\ -0.0404 & -0.3213 & -0.2891 & 0 & 0\\ 0 & 0 & 1 & 0 & 0\\ 0 & -1 & 0 & 15 & 0\end{bmatrix} \qquad B_{long} = \begin{bmatrix} 0 & 1\\ 2.0212 & 0\\ -0.8456 & 0\\ 0 & 0\\ 0 & 0\end{bmatrix}$$

$$A_{latr} = \begin{bmatrix} -0.3668 & 0 & -15.0921 & 9.81 & 0\\ -1.8845 & -6.7094 & 3.012 & 0 & 0\\ 1.9533 & -0.1943 & -4.0090 & 0 & 0\\ 0 & 1 & 0 & 0 & 0\\ 0 & 0 & 1 & 0 & 0\end{bmatrix} \qquad B_{latr} = \begin{bmatrix} 0 & -0.9545\\ 22.6176 & 27.6471\\ 9.0346 & -2.1004\\ 0 & 0\\ 0 & 0\end{bmatrix}$$

This state-space model will be used for the control design in Section 2.3.

2.3 Fixed-Wing Control

Linear Quadratic Control (LQR) was chosen to conduct the control design for the fixed-wing UAV. LQR was chosen for the fixed-wing control design as it provides an optimal solution with robust stability. It was implemented in MATLAB using the following built-in function:

```
[K,S,CLP]=lqr(SYS,Q,R)
```

where K is the gain matrix, SYS is the state-space model, S is the solution to the Riccati equation, and CLP represents the closed-loop poles. This approach was used for both

longitudinal and lateral state-space models. *Q* and *R* were tuned using trial and error, and Table 2-1 shows the final values that were used for each model.

Parameter	Q	R
Longitudinal	1	0.01
Lateral	1	0.1

Table 2-1: Q and R Parameters

The chosen *Q* and *R* values yielded the following matrices for *K*:

$$K_{long} = \begin{bmatrix} 5.8347 & 7.2621 & -49.9416 & -211.1728 & -11.5380 & 9.6010 & 1.5323 & -8.4033 & 5.4207 \\ 32.0312 & -17.9177 & -48.3846 & 2.03242 & 23.0346 & 0.0438 & 16.9686 & -5.4207 & -8.4033 \end{bmatrix}$$

$$K_{latr} = \begin{bmatrix} -1.2765 & 1.3361 & 4.2063 & 1.6096 & 9.9830 & 3.1987 & 0.3550 & 1.7663 & -2.6230 \\ 1.1063 & 2.3862 & -2.5354 & 8.1738 & 3.2899 & 0.3550 & 3.2224 & -2.6230 & -1.7663 \end{bmatrix}$$

2.4 Fixed-Wing Simulation

The dynamics developed in Section 2.2 and the control gains determined in Section 2.3 were used to build the simulation model in Simulink. Figure 2-3 shows the main control subsystem, divided into a longitudinal path and a lateral path. Each path takes in commands from input ports 1 to 4. The commands are multiplied by tracking gains and are also summed with state feedback gains and input gains. The inputs are then passed through actuator dynamics transfer functions for the elevator, throttle, aileron, and rudder, and are then fed into state-space blocks through output ports 1 to 4. Moreover, since the UAV needs to perform manoeuvres at certain distances in the north Earth reference frame direction, a tracking function was implemented with the Earth reference frame north velocity equation:

$$\dot{p}_n = (cos\theta cos\psi)u + (sin\phi sin\theta cos\psi - cos\phi sin\psi)v + (cos\phi sin\theta cos\psi + sin\phi sin\psi)w \quad [3]$$

This equation was integrated over time to obtain the Earth reference frame north position at the current timestep. This result was fed into a MATLAB logic function which would decide what commands to output based on the current position and heading.

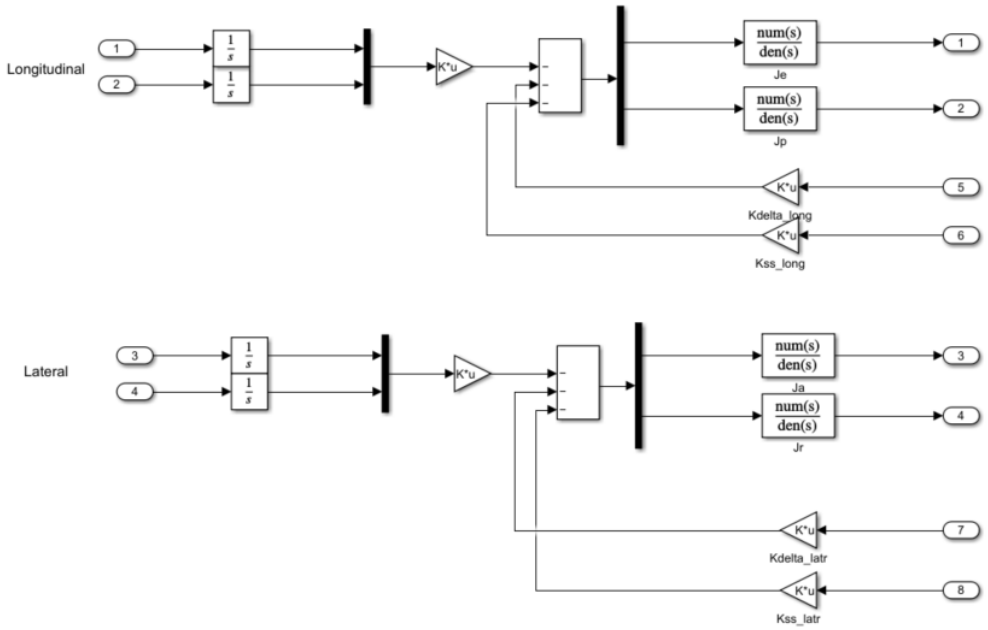

Figure 2-3: Fixed-Wing Control Subsystem

The simulation was run, and the plots in Figure 2-4 were obtained, showing the altitude, roll angle, and heading of the UAV. As can be seen, the UAV is able to execute the ascent to 2000 m, the 180° turn, and the descent back to 2000 m. However, the manoeuvres are executed at unrealistic speeds and an unrealistic turn radius. This may be due to lack of saturation on the input commands as well as tuning inaccuracies.

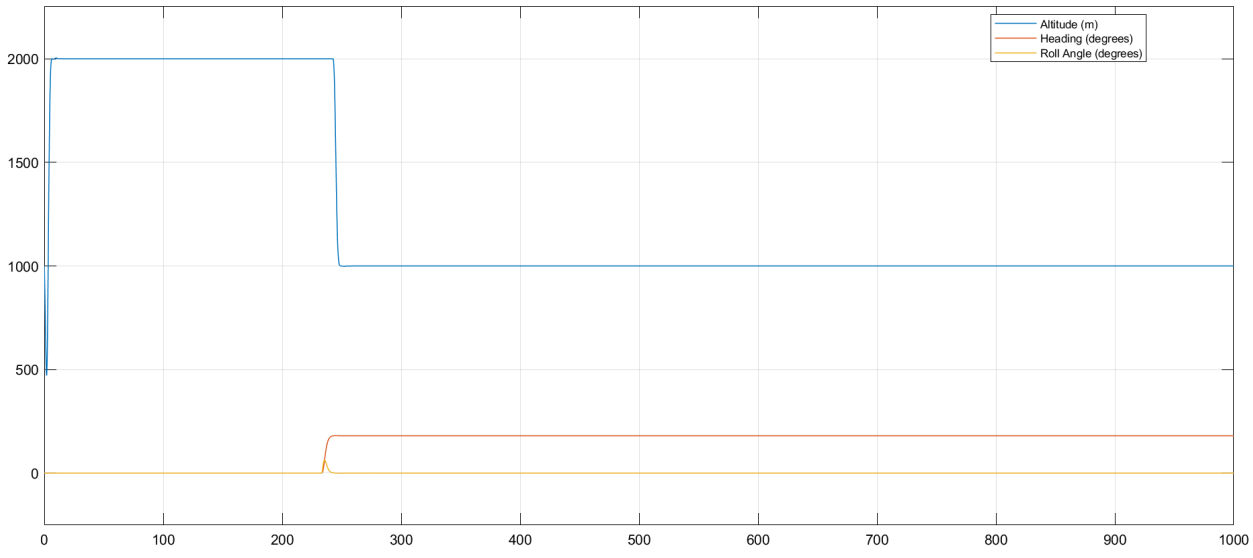

Figure 2-4: Fixed Wing Simulation Results

3.0 Multi-Rotor Drone Development

A study was conducted which modelled and simulated a quadrotor drone flying along a desired trajectory using MATLAB and Simulink. The maximum range and endurance performance was first calculated for this UAS. Furthermore, a controller was developed to execute a set of commands for the quadrotor to fly to and hover at a set of desired locations. The dynamics model and position estimation was first developed, and then the aforementioned controller was developed to control the drone's location in 3D space and its yaw.

3.1 Multi-Rotor Range and Endurance

The maximum range and endurance for a quadrotor drone was calculated using MATLAB. The drone is electric and stores energy in a battery to power four motors. Using forward flight-momentum theory and a 0th order battery model, the range and endurance can be calculated. Forward flight momentum theory can be used to calculate the amount of power needed to spin a propeller at a defined velocity. The model finds the induced velocity of the propeller at an angled flight to calculate the total power. The 0th order battery model assumes constant efficiencies and voltages as the energy in the battery is used. As a result the total energy in the battery can be assumed to equal the total voltage times the capacity of the battery. Since the voltage is assumed to remain constant, the motor and ESC efficiency is constant. Therefore the time of flight and range can be found using the formulas below.

$$t = \frac{E_b \eta_m \eta_e}{P_{prop}}, \quad d = vt = v * \left(\frac{E_b \eta_m \eta_e}{P_{prop}}\right) = \left(\frac{v}{P_{prop}}\right) E_b \eta_m \eta_e$$

To find the maximum endurance, the speed that provides the least power would be required and for the maximum range, the speed that provides the smallest ratio of power over velocity would be required. To find these values, the power is calculated at a range of velocities between 0 and 20 m/s in increments of 0.5 m/s. A plot of the results are shown in Figure 3-1. Using this method, the results show that the max endurance is 68.1 min at a speed of 7 m/s and the max range is 36.061 km at a speed of 9.5 m/s.

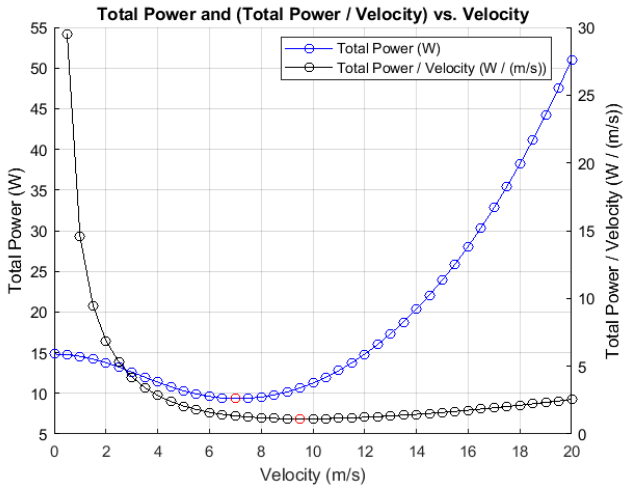

Figure 3-1: Total power and (Total power / Velocity) vs Velocity plot

This result is a theoretical calculation and may be different from what is measured in practice. The pilot may now be able to constantly maintain the speed required, and additional power would be needed to adjust for altitude change and other disturbances. Furthermore, the 0th order battery model is only an approximation of the usable energy in the battery.

3.2 Multi-Rotor Dynamics

The dynamics model for the multi-rotor was developed through a set of state-space model relationships provided in the assignment handout. Table 3-1 below lists the inputs and outputs for each of these state-space models.

Name	Input	Output
Roll	Desired roll angle	Actual roll angle
Pitch	Desired pitch angle	Actual pitch angle
Yaw	Desired yaw rate in rad/s	Actual yaw angle in rad
Height	Desired vertical speed in m/s	Actual height in m
Pitch to u	Actual pitch angle	Actual forward velocity in body frame (u)
Roll to v	Actual roll angle	Actual sideways velocity in body frame (v)

Table 3-1: State-Space Inputs and Outputs Used For Dynamics Model

Using the state-space blocks in Simulink and the parameters provided in the project instructions, the dynamics model from input (left), to output (right) was implemented as shown in Figure 3-2.

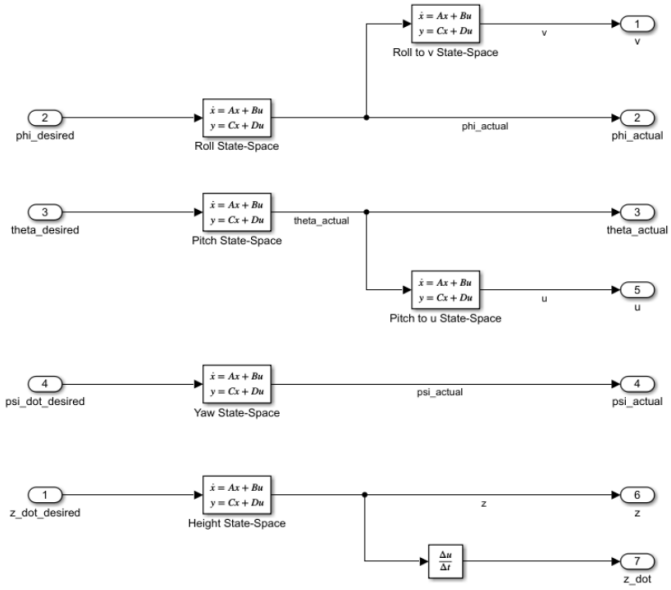

Figure 3-2: Dynamics Model Implementation

3.3 Multi-Rotor Position Estimation

The position estimation for the model uses the output of the dynamics model in order to calculate positions x, y, and Euler angle first derivatives p, q, and r. Positions x and y are calculated according to equation 3.1 of [3]. As inputs, this equation uses Euler angles ϕ, θ, and ψ, as well as body frame linear velocities u and v, all of which are outputs of the dynamics model. Based on these inputs, linear velocities in the inertial frame $\dot{x}$ and $\dot{y}$ are calculated. These are then integrated to calculate positions x and y.

Additionally, the body frame angular velocities p, q, and r are calculated according to the equation on slide 5 of Lecture 9 - Part III [4]. As inputs, this equation takes in the Euler angles outputted by the dynamics model, as well as their first derivatives.

Figure 3-3 shows how the position estimation was implemented in Simulink, with inputs shown on the left, and outputs shown on the right. Within the diagram, there are several subsystem blocks to simplify intermediate calculations for the equations described above.

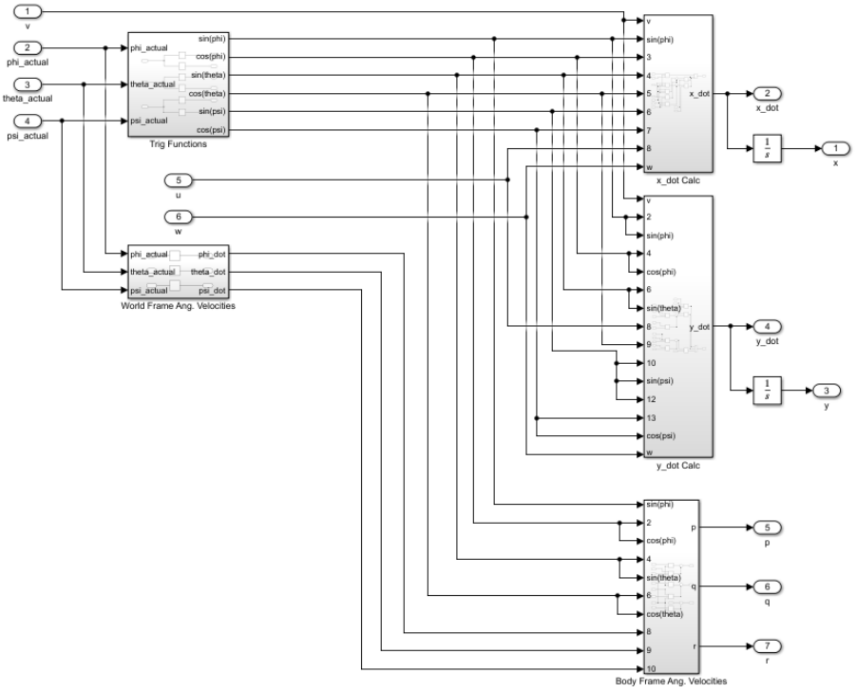

Figure 3-3: Position Estimation Implementation

3.4 Multi-Rotor Position Control

Based on both the dynamics and position estimation models, it is possible to obtain actual values of positions x, y, and z; Euler angles ϕ, θ, and ψ; and any of their derivatives. Given this information, as well as desired positions and yaw, linear controllers can be designed to have the multi-rotor fly along a desired trajectory.

For x, z, and ψ, PD control equations as described in slides 20, 25, and 22 of Lecture 9 - Part III respectively were used in order to calculate the controlling $\ddot{x}$, $\ddot{z}$, and ψ [4]. For the $\ddot{y}$ control however, a PID controller was implemented rather than a PD controller in order to use integral control as a way to reduce steady state error. The implementation of this is shown in Figure 3-4. The corresponding control diagrams for $\ddot{x}$, $\ddot{z}$, and ψ (for yaw control) are similar, but without the integral control branch. Finally, based on the controlling $\ddot{x}$, $\ddot{z}$, and ψ, the controlling Euler angles ϕ and θ can be calculated as described in slide 22 of Lecture 9 - Part III [4]. The Simulink implementation of the position controller is shown in Figure 3-5, and Figure 3-4 corresponds to one of the 3 blocks in the Lin. Acc. Control subsystem within Figure 3-5.

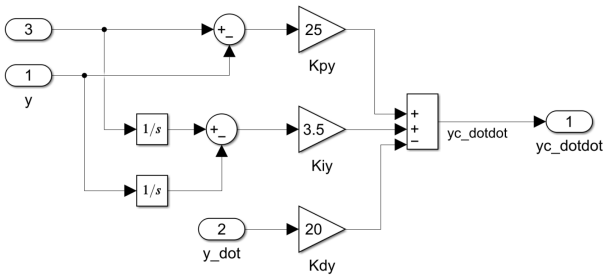

Figure 3-4: PID Control of y position in Simulink

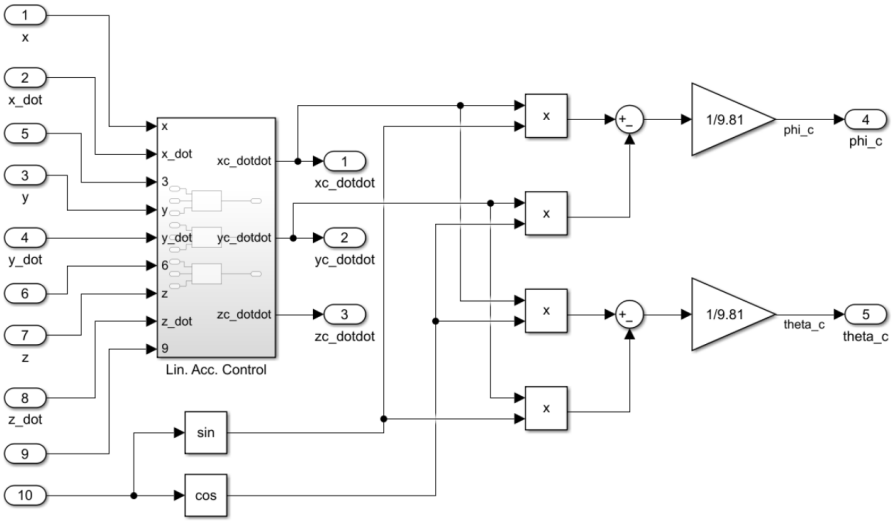

Figure 3-5: Position Control Implementation

The tuning process for each controller was done manually through an iterative process. Generally, this process consisted of first only increasing K_p while the system response was stable, then increasing K_d to dampen the system and try to increase response time. Each parameter was then adjusted individually as needed in order to speeden response time or reduce oscillations. The final PID gains chosen are presented in Appendix E.

After implementing the position and yaw controllers, relevant outputs are fed into the input of the dynamics model in order to close the feedback loop.

3.5 Multi-Rotor Results

The results of the Simulink model and simulation are shown in Figure 3-6, and the entire Simulink model is shown in Appendix F. The dashed lines show the desired x, y, and z positions passed to the position controller as inputs (input ports 5, 6, and 9 in Figure 3-5), and the solid lines show the actual position of the multi-rotor. The trajectory shown in Figure 3-6 corresponds to what was described in the project instructions, but the position inputs can be changed and a similar quality of results can be achieved.

In the z direction, the response most closely matches the input signal. In the x direction, the response generally follows the input, but the response is clearly overdamped. During the tuning process, this was intentionally chosen over having a faster response with more oscillations and overshoot. This is because given the lack of explicit design criteria, it was assumed that the former would be perceived as "smoother," and also because in a real-life system, oscillations would be undesirable from both a structural and maintenance standpoint. In the y direction, which was the most difficult to tune and required adding integral control to remove steady-state error, there is some overshoot in the second half of the simulation. Unfortunately, it was difficult to find a set of PID gains to completely remove this overshoot.

A key assumption that should be mentioned for these results, and for results where the x, y, and z positions are chosen differently from those shown here, is that ψ be approximately 0. This is because linear control theory has been used to design these controllers around the set point of $\psi_c = 0$. If values that are not approximately zero are used, then the linearization of the $\sin(\psi_c)$ and $\cos(\psi_c)$ terms in the ϕ_c and θ_c equations (slide 22 of Lecture 9 - Part III) does not hold, and the results become unstable.

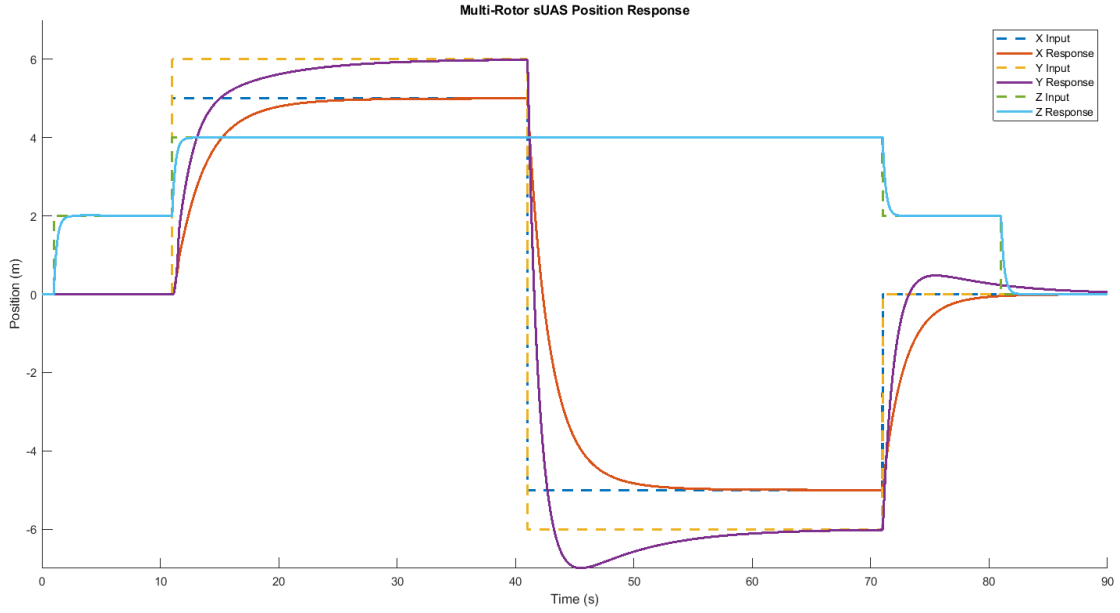

Figure 3-6: Multi-Rotor Simulation Results

4.0 Conclusions and Lessons Learned

In conclusion, simulations and modelling on MATLAB and simulink were conducted on a fixed-wing Aerosonde UAV and a quad-rotor drone configuration to understand their performance and develop a control algorithm. Range and endurance estimates were calculated for both sUAS configurations. Information about the engine, plane, and propeller was used to find the optimal power and fuel consumption. Numerical integration was used to determine that the max endurance is 65.1 hr and the max range is 4034 km. This was determined to be too large due to inaccurate representations of the engine. The multi-rotor range and endurance is also calculated to be 34.061 km at a speed of 9.5 m/s and 68.1 min at a speed of 7 m/s respectively, using a 0th order battery model and forward flight momentum theory.

A control model was developed and tested for the fixed wing UAV to perform a set of manoeuvres. A linear state-space dynamics model and an LQR controller were integrated into a control system to perform altitude control and a level-coordinated turn. The controller was able to perform the tasks but with unrealistic oscillations and spikes that require further optimization. A control model was also developed for a quadcopter to fly the drone to specific locations and hover. A linear dynamics model, position estimation, and a PID controller were used in a control system to execute several commands. The results show that the drone was able to successfully perform the tasks with reasonable results.

One of the major lessons learned in this study was that when trying to optimise the controller for one parameter, it usually resulted in a trade-off of another. For example, reducing the settling time may increase undesired effects such as overshoot or steady-state error.

The roles of the team are as follows: David developed the fixed-wing range and endurance, and assisted with fixed-wing control design and multi-rotor range and endurance, Shahzeb led the design of the fixed-wing control system, and Farhan led the multi-rotor control development.

References

[1] "UIUC PDB - Vol 3." [Online]. Available: https://m-selig.ae.illinois.edu/props/volume-3/propDB-volume-3.html. [Accessed: 15-Dec-2021]

[2] "EL-005 Engine." [Online]. Available: https://www.lycoming.com/engines/el-005. [Accessed: 15-Dec-2021]

[3] R. W. Beard and T. W. Mclain, *Small Unmanned Aircraft - Theory and Practice*. Princeton, NJ, USA: Princeton University Press, 2012.

[4] K. Pereida, T. Bamford, and A. Schoellig, "Lecture 13 - Quadrotor Dynamics and Control III," Nov-2020 [Online]. Available: https://q.utoronto.ca/courses/242508/pages/course-contents. [Accessed: 19-Dec-2021]

[5] H. H. T Liu, *ANALYTICAL AIRCRAFT FLIGHT*. 2021.

Appendix

Appendix A - CT and CP vs. J Curve Estimates

To build a function to relate the CT and CP values of the prop with respect to the J value, curves of best fit were applied to the provided data of the prop. A quadratic curve was applied to the CT values and an exponential model was used for CP to minimise the error in the curve fits. Examples are shown in Figures A-1 and A-2

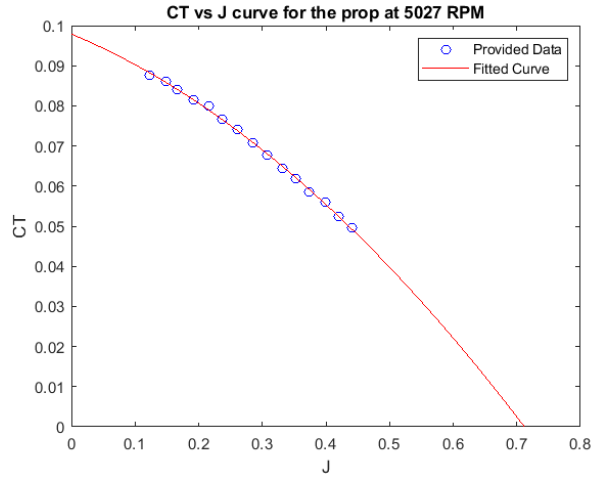

Figure A-1: CT vs. J Curve of Best Fit

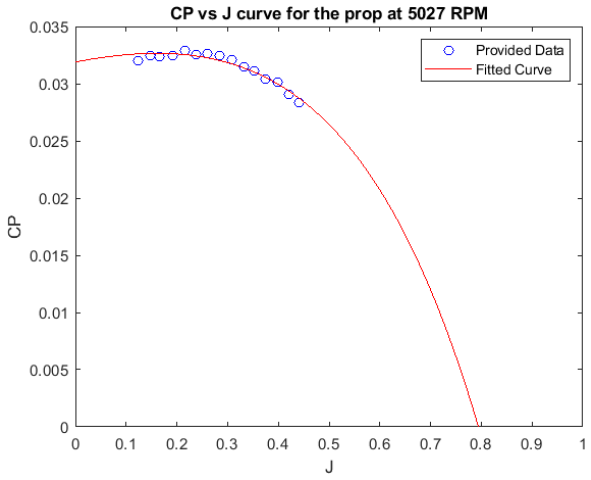

Figure A-2: CP vs. J Curve of Best Fit

Appendix B - Fuel Consumption vs. Velocity

To find the optimal velocity to fly at, for each weight increment, the relationship between the fuel consumption vs. velocity and the fuel consumption over velocity vs. velocity was determined. The velocities that provide the minimal values were used. Figures B-1 and B-2 show an example of this relationship for the initial weight.

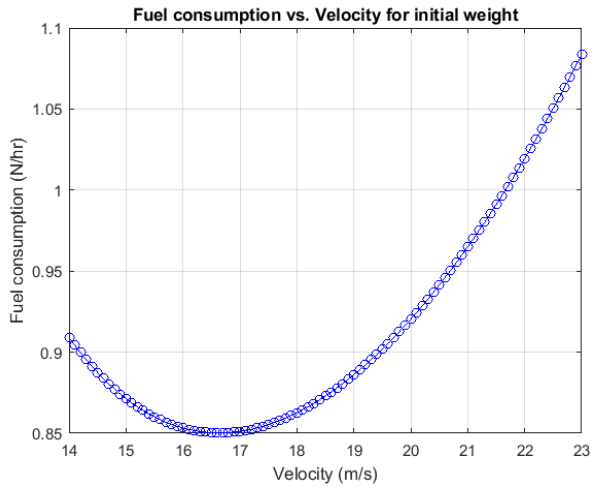

Figure B-1: Fuel Rate vs. Velocity

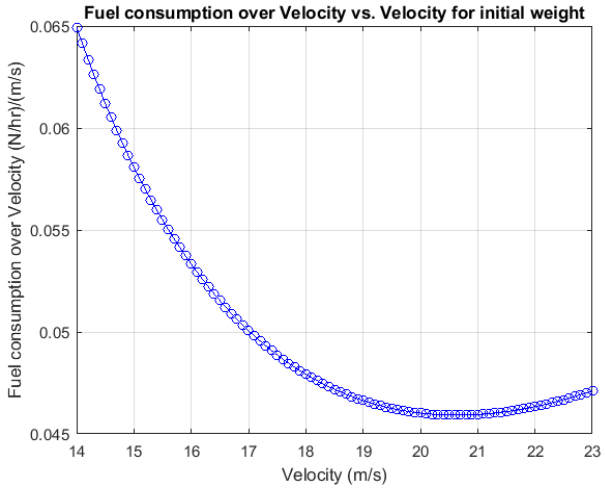

Figure B-2: Fuel Rate over Velocity vs. Velocity

Appendix C - Aerodynamic and Control Derivatives

Longitudinal	*Formula*
X_u	$\frac{u^*\rho S}{\mathrm{m}}\left[C_{X_0}+C_{X_\alpha}\alpha^*+C_{X_{\delta_e}}\delta_e^*\right]-\frac{\rho S w^* C_{X_\alpha}}{2\mathrm{m}}+\frac{\rho S c C_{X_q} u^* q^*}{4mV_a^*}-\frac{\rho S_{\mathrm{prop}} C_{\mathrm{prop}} u^*}{\mathrm{m}}$
X_w	$-q^*+\frac{w^*\rho S}{\mathrm{m}}\left[C_{X_0}+C_{X_\alpha}\alpha^*+C_{X_{\delta_e}}\delta_e^*\right]+\frac{\rho S c C_{X_q} w^* q^*}{4mV_a^*}+\frac{\rho S C_{X_\alpha} u^*}{2\mathrm{m}}-\frac{\rho S_{\mathrm{prop}} C_{\mathrm{prop}} w^*}{\mathrm{m}}$
X_q	$-w^*+\frac{\rho V_a^* S C_{X_q} c}{4\mathrm{m}}$
X_{δ_e}	$\frac{\rho V_a^{*2} S C_{X_{\delta_e}}}{2\mathrm{m}}$
X_{δ_t}	$\frac{\rho S_{prop} C_{prop} k^2 \delta_t^*}{\mathrm{m}}$
Z_u	$q^*+\frac{u^*\rho S}{\mathrm{m}}\left[C_{Z_0}+C_{Z_\alpha}\alpha^*+C_{Z_{\delta_e}}\delta_e^*\right]-\frac{\rho S C_{Z_\alpha} w^*}{2\mathrm{m}}+\frac{u^*\rho S C_{Z_q} c q^*}{4mV_a^*}$
Z_w	$\frac{w^*\rho S}{\mathrm{m}}\left[C_{Z_0}+C_{Z_\alpha}\alpha^*+C_{Z_{\delta_e}}\delta_e^*\right]+\frac{\rho S C_{Z_\alpha} u^*}{2\mathrm{m}}+\frac{\rho w^* S c C_{Z_q} q^*}{4mV_a^*}$
Z_q	$u^*+\frac{\rho V_a^* S C_{Z_q} c}{4\mathrm{m}}$
Z_{δ_e}	$\frac{\rho V_a^{*2} S C_{Z_{\delta_e}}}{2\mathrm{m}}$
M_u	$\frac{u^*\rho S c}{J_y}\left[C_{m_0}+C_{m_\alpha}\alpha^*+C_{m_{\delta_e}}\delta_e^*\right]-\frac{\rho S c C_{m_\alpha} w^*}{2J_y}+\frac{\rho S c^2 C_{m_q} q^* u^*}{4J_y V_a^*}$
M_w	$\frac{w^*\rho S c}{J_y}\left[C_{m_0}+C_{m_\alpha}\alpha^*+C_{m_{\delta_e}}\delta_e^*\right]+\frac{\rho S c C_{m_\alpha} u^*}{2J_y}+\frac{\rho S c^2 C_{m_q} q^* w^*}{4J_y V_a^*}$
M_q	$\frac{\rho V_a^* S c^2 C_{m_q}}{4J_y}$
M_{δ_e}	$\frac{\rho V_a^{*2} S c C_{m_{\delta_e}}}{2J_y}$

[3]

Lateral	*Formula*
Y_v	$\frac{\rho Sbv^*}{4mV_a^*}[C_{Y_p}p^* + C_{Y_r}r^*] + \frac{\rho Sv^*}{\mathrm{m}}\left[C_{Y_0} + C_{Y_\beta}\beta^* + C_{Y_{\delta_a}}\delta_a^* + C_{Y_{\delta_r}}\delta_r^*\right]$
	$+\frac{\rho SC_{Y_\beta}}{2\mathrm{m}}\sqrt{u^{*2} + w^{*2}}$
Y_p	$w^* + \frac{\rho V_a^* Sb}{4m}C_{Y_p}$
Y_r	$-u^* + \frac{\rho V_a^* Sb}{4m}C_{Y_r}$
Y_{δ_a}	$\frac{\rho V_a^{*2} S}{2\mathrm{m}}C_{Y_{\delta_a}}$
Y_{δ_r}	$\frac{\rho V_a^{*2} S}{2\mathrm{m}}C_{Y_{\delta_r}}$
L_v	$\frac{\rho Sb^2v^*}{4V_a^*}[C_{p_p}p^* + C_{p_r}r^*] + \rho Sbv^*[C_{p_0} + C_{p_\beta}\beta^* + C_{p_{\delta_a}}\delta_a^* + C_{p_{\delta_r}}\delta_r^*]$
	$+\frac{\rho SbC_{p_\beta}}{2}\sqrt{u^{*2} + w^{*2}}$
L_p	$\Gamma_1 q^* + \frac{\rho V_a^* Sb^2}{4}C_{p_p}$
L_r	$-\Gamma_2 q^* + \frac{\rho V_a^* Sb^2}{4}C_{p_r}$
L_{δ_a}	$\frac{\rho V_a^{*2} Sb}{2}C_{p_{\delta_a}}$
L_{δ_r}	$\frac{\rho V_a^{*2} Sb}{2}C_{p_{\delta_r}}$
N_v	$\frac{\rho Sb^2v^*}{4V_a^*}\left[C_{r_p}p^* + C_{r_r}r^*\right] + \rho Sbv^*[C_{r_0} + C_{r_\beta}\beta^* + C_{r_{\delta_a}}\delta_a^* + C_{r_{\delta_r}}\delta_r^*]$
	$+\frac{\rho SbC_{r_\beta}}{2}\sqrt{u^{*2} + w^{*2}}$
N_p	$\Gamma_7 q^* + \frac{\rho V_a^* Sb^2}{4}C_{r_p}$
N_r	$-\Gamma_1 q^* + \frac{\rho V_a^* Sb^2}{4}C_{r_r}$
N_{δ_a}	$\frac{\rho V_a^{*2} Sb}{2}C_{r_{\delta_a}}$
N_{δ_r}	$\frac{\rho V_a^{*2} Sb}{2}C_{r_{\delta_r}}$

[3]

Appendix D - Linear Quadratic Regulator Theory

Consider the state-space system in the form:

$$\dot{x} = Ax + Bu$$
$$u = -Kx$$

LQR outputs the optimal state feedback gain, *K*, based on the Linear Quadratic Performance Index:

$$J = \frac{1}{2}\int_0^\infty (x^T Q x + u^T R u) dt$$

where the *Q* matrix is the weight on the states while the *R* matrix is the weight on the control input. *K* is computed as follows:

$$K = R^{-1} B^T P$$

where the constant *P* satisfies the algebraic Riccati equation:

$$PA + A^T P - PBR^{-1}B^T P + Q = 0, P = P^T$$

[5]

Appendix E - Multi-Rotor PID Gains

Table E-1 presents the PID gains chosen for the position and yaw controllers.

State	P	I	D
x	20	-	35
y	25	3.5	20
z	30	-	8
ψ	10	-	0.01

Table E-1: PID Gains for Position and Yaw Control

Appendix F - Simulink Models

Refer to Figure F-1 for a diagram of the entire Fixed-Wing Simulink model:

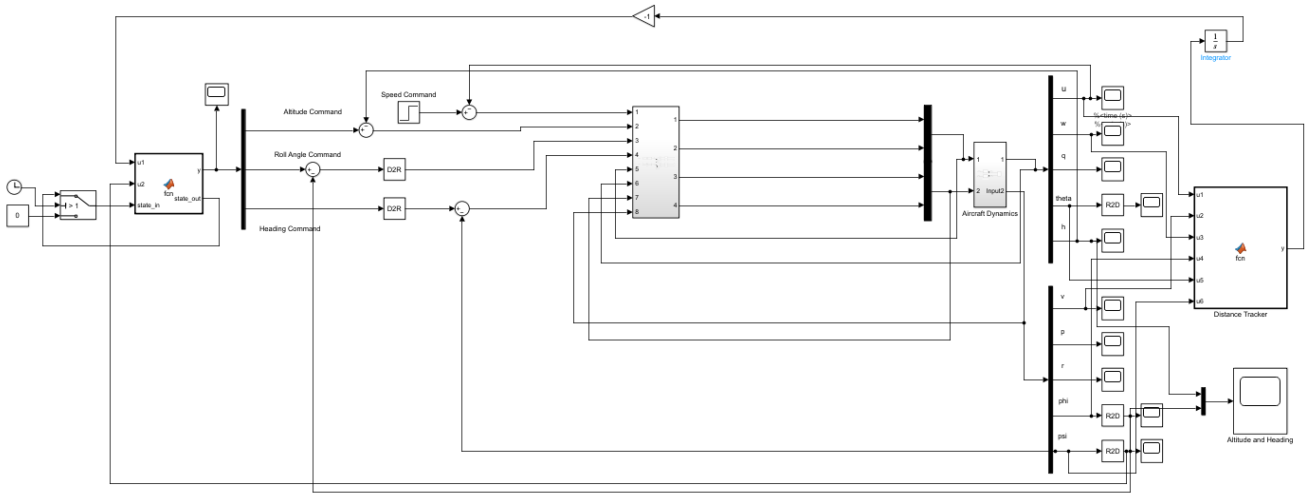

Figure F-1: Fixed-Wing Simulink Model

Refer to Figure F-2 for a diagram of the entire Multi-Rotor Simulink model:

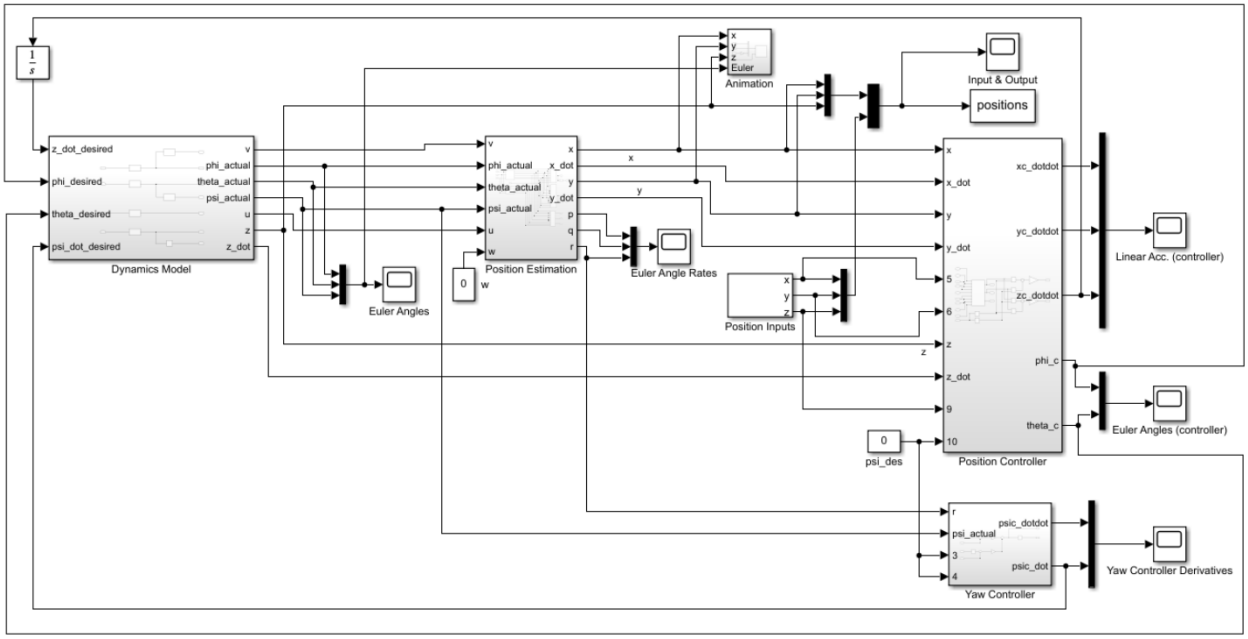

Figure F-2: Multi-Rotor Simulink Model